Investigating the differential abscopal effects based on tumor immunogenicity and its implications for enhancing radiotherapy efficacy

Yoon Seok Jeong

The Graduate School
Yonsei University
Department of Medicine

Investigating the differential abscopal effects based on tumor immunogenicity and its implications for enhancing radiotherapy efficacy

A Master's Thesis Submitted
to the Department of Medicine
and the Graduate School of Yonsei University
in partial fulfillment of the
requirements for the degree of
Master of Medical Science

Yoon Seok Jeong

December 2024

This certifies that the Master's Thesis of Yoon Seok Jeong is approved

Thesis Supervisor Kyung Hwan Kim

Thesis Committee Member Nam Suk Sim

Thesis Committee Member Hyunsoo Cho

The Graduate School
Yonsei University
December 2024

ACKNOWLEDGEMENTS

This study was supported by a faculty research grant of Yonsei University College of Medicine (6-2021-0111) and National Research Foundation (NRF) grant (NRF-2021R1I1A1A01044024).

TABLE OF CONTENTS

LIST OF FIGURES ii
ABSTRACT iii
1. INTRODUCTION 1
2. MATERIALS AND METHODS 4
2.1. Cell lines 4
2.2. Mouse experiments 4
2.2.1. Comparison of immunogenicity between B16F10 and B16-OVA tumor 4
2.2.2. B16F10 and B16-OVA abscopal mouse model 5
2.2.3. FTY720 and anti-CD8α treatment in mouse model 5
2.3. Immunofluorescence 6
2.4. Flow cytometry 7
2.5. TCR sequencing analysis 8
2.6. Statistic analysis 8
3. Result 10
3.1. B16-OVA exhibits the characteristics of a more immunogenic tumor compared to B16F10 10
3.2. The abscopal effect is associated with the immunogenicity of the primary tumor 10
3.3. Increased T cell infiltration and function in the B16-OVA abscopal model 16
4. DISCUSSION 22
5. CONCLUSION 26
REFERENCES 28
ABSTRACT IN KOREAN 31

LIST OF FIGURES

Fig 1. Gating strategy for identifying T cell, DC, TAM subpopulations ·····9
Fig 2. Number and phenotype of T cell populations in B16F10 tumors and B16-OVA tumors·····12
Fig 3. Experimental schedule and tumor size comparison graphs of IR and non-IR tumors following IR of tumors with differing immunogenicity in an abscopal model·····14
Fig 4. Flow cytometry analysis of T cell number and phenotype of secondary and primary tumors·····18
Fig 5. Flow cytometry analysis of cytokine production in secondary tumor. ·····20

ABSTRACT

Investigating the differential abscopal effects based on tumor immunogenicity and its implications for enhancing radiotherapy efficacy

The abscopal effect, enhancing antitumor responses through ionizing radiation (IR), is influenced by tumor immunogenicity—the ability of tumors to elicit immune responses suppressing growth. This study examined the role of tumor immunogenicity in the abscopal effect using B16F10 (low immunogenicity) and B16-OVA (high immunogenicity) models in C57BL/6 mice. Flow cytometry and immunofluorescence revealed higher $CD8^+$ T cell frequencies and greater T cell infiltration in B16-OVA tumors, along with increased Granzyme B^+ ($GzmB^+$), Ki-67^+, and PD-1^+ $CD8^+$ T cells. B16-OVA tumors also exhibited elevated $CD40^+$ and $CD86^+$ dendritic cells (DCs) and reduced PD-$L1^+$ tumor-associated macrophages (TAMs), indicating a more immunogenic tumor microenvironment (TME). The B16-OVA abscopal model exhibited a more pronounced abscopal effect compared to the B16F10 model, with greater secondary tumor growth delay following IR, particularly under αPD-1 treatment. Mechanistic studies using FTY720 and $CD8^+$ T cell depletion confirmed $CD8^+$ T cells drive systemic antitumor responses and the abscopal effect. Secondary tumors in the IR-treated B16-OVA αPD-1 group showed increased T cell infiltration, elevated $GzmB^+$ $CD8^+$ T cells, and higher levels of terminally differentiated TCF-1^- TIM-3^+ $CD8^+$ PD-1^+ T cells, indicative of cytotoxic populations. Polyfunctional $CD8^+$ T cells co-expressing IFN-γ, TNF-α, and IL-2, along with polyfunctional $CD4^+$ T cells, were significantly elevated in the B16-OVA model. This study highlights tumor immunogenicity as a key determinant of the abscopal effect, with enhanced infiltration, functionality, and polyfunctionality of T cells as critical mechanisms. Combining IR with immune checkpoint inhibitors (ICIs) targeting tumor immunogenicity optimizes systemic antitumor responses and improves outcomes.

Key words : Abscopal effect, Immunogenicity, Ionizing Radiation

1. INTRODUCTION

Ionizing radiation (IR) induces cancer cell death while also enhancing immune responses by altering the tumor microenvironment.[1] A key mechanism is immunogenic cell death, which releases damage-associated molecular patterns to activate antigen-presenting cells (APCs), driving T cell responses and immunological memory.[2] IR also activates the cGAS-STING pathway, which triggers the production of Type I interferons, bridging innate and adaptive immunity, and increases MHC I expression to enhance tumor-specific immune responses.[3,4] Additionally, IR-induced DNA damage can generate mutations that lead to the presentation of tumor neoantigens, boosting $CD8^+$ and $CD4^+$ T cell responses and strengthening tumor control.[5] Acting as an in situ vaccination, IR promotes antitumor immunity, though its efficacy is highly dependent on $CD8^+$ T cells.[6,7] Interestingly, the immune responses induced by IR are not limited to the IR site but can extend systemically, leading to the regression of distant, non-IR tumors, a phenomenon known as the abscopal effect.[8] This phenomenon highlights the systemic nature of the immune response, wherein the release of tumor antigens from the IR tumor and the subsequent activation of T cells can lead to the recognition and elimination of distant tumor cells.[9] The abscopal effect is mediated by multiple mechanisms, including immunogenic cell death, which releases tumor-associated antigens and damage-associated molecular patterns that stimulate APCs. Activated APCs, in turn, prime and expand tumor specific T cells, enabling the immune system to target non-IR tumors.[10] Understanding the mechanisms underlying the abscopal effect has significant clinical implications, offering opportunities to develop combination therapies that integrate IR with immune checkpoint inhibitors (ICIs), which synergize by enhancing T cell activation and overcoming immune suppression.

In preclinical models, the abscopal effect is frequently observed, with robust systemic antitumor responses and regression of distant, non-irradiated tumors when localized IR is combined with ICIs.[11] However, in clinical settings, the abscopal effect is rarely observed, likely due to the complexity and heterogeneity of the tumor microenvironment (TME) and the insufficient systemic immune activation achieved by IR alone.[8] Clinical trials rarely achieve significant abscopal effects or improvements in outcomes such as overall response rate and progression-free survival,

highlighting the challenges of translating preclinical success into clinical practice.[12] This discrepancy may stem from differences in the TME between controlled preclinical models and patient-specific contexts. Recent advancements emphasize the need to understand patient-specific immune landscapes and develop sophisticated translational approaches to bridge this gap and optimize therapeutic outcomes.[13] Given the rarity of the abscopal effect in clinical settings, recent strategies have focused on combining IR with ICIs, such as αPD-1 (Anti-Programmed Death-1) or αPD-L1 (Anti-Programmed Death-Ligand 1), to enhance systemic immune activation and overcome the limitations imposed by the TME.[14,15] IR alone rarely induces the abscopal effect due to the immunosuppressive nature of the TME, characterized by regulatory T cells (Tregs), tumor-associated macrophages (TAMs), and the IR-induced upregulation of immune checkpoint molecules like PD-L1. These factors suppress systemic immune activation, necessitating combination approaches to counteract these barriers and promote anti-tumor immunity.[16,17] Recent preclinical findings highlight the importance of treatment sequencing in achieving robust abscopal responses. Administering ICIs, such as anti-PD-1, after localized tumor irradiation optimizes abscopal antitumor immune responses by promoting polyfunctional $CD8^+$ T cell activation and reducing tumor volumes at both IR and non-IR sites.[18] Despite promising results in preclinical models, the abscopal effect observed with IR and ICIs has been rare and inconsistent in clinical settings, highlighting a significant gap in our understanding. While factors such as the complexity of the human TME and treatment variability are thought to contribute, the precise mechanisms underlying this disparity between preclinical and clinical outcomes remain incompletely elucidated.

In preclinical studies investigating the abscopal effect induced by combining IR with ICIs, the focus has primarily been on treating one or a subset of lesions while measuring the size of non-IR tumors. In clinical studies, the choice of the IR tumor has often been left to the discretion of the treating physician, an approach that has been shown to be suboptimal. Recognizing these methodological limitations, we hypothesized that the immunogenicity of the irradiated tumor plays a critical role in eliciting the abscopal effect. Previous studies have provided preclinical evidence supporting the role of tumor immunogenicity in the abscopal effect. For instance, one study demonstrated that highly immunogenic MC38 tumors exhibited a stronger abscopal effect compared to less immunogenic 4T1 tumors, correlating with differences in $CD8^+$ T cell activation and systemic

immune responses. However, the use of tumor types with entirely distinct genomic and biological properties limited the ability to precisely isolate the impact of tumor immunogenicity on the abscopal effect. To address this gap, we utilized tumor models with identical genomic backgrounds but differing in the expression of an external antigen. Specifically, we compared the abscopal effects between B16 tumors and the more immunogenic B16-OVA tumors. Our findings revealed that B16-OVA tumors exhibited a stronger abscopal effect compared to B16 tumors, characterized by increased $CD8^+$ T cell infiltration, elevated expression of effector molecules such as Granzyme B, IFN-γ, TNF-α, and IL-2, and enhanced polyfunctionality of immune responses in secondary tumors. These results underscore the pivotal role of tumor immunogenicity in driving systemic antitumor responses through the abscopal effect and highlight the importance of considering tumor immunogenicity when designing therapeutic strategies involving IR and ICIs.[19]

2. Materials and Methods

2.1. Cell lines

In this study, the B16F10 and B16-OVA tumor cells were utilized. The B16-OVA tumor cells are modified version of the B16F10 tumor cells, engineered to express the egg white protein ovalbumin(OVA), thereby serving as a model for investigating T cell antigen recognition. B16F10 tumor cells were purchased from the American Type Culture Collection. B16-OVA tumor cells were generously provided by Dr. Sang-Jun Ha from Yonsei University. Both tumor cells were cultured in Dulbecco's modified Eagle's medium (DMEM) supplemented with 10% fetal bovine serum (FBS) and 1% penicillin-streptomycin (P/S). The tumor cells were maintained at 37°C in a humidified atmosphere containing 5% CO_2.

2.2. Mouse experiments

Female C57BL/6 mice (age 5-6 weeks) were purchased from Orient Bio. Prior to the initiation of the experiment, the animals were acclimated for a period of one week to minimize any stress-related variables that could potentially affect the outcomes of the study. All experimental procedures were performed in accordance with institutional guidelines and were approved by the relevant ethics committee. All animal procedures were approved by the Institutional Animal Care and Use Committee (IACUC) of Yonsei University (IACUC-2023-0134).

2.2.1. Comparison of immunogenicity between B16F10 and B16-OVA tumor

C57BL/6 mice were divided into two groups for the study. One group was injected subcutaneously in the left thigh with 100 μL of DPBS containing 0.5×10^6 B16-OVA tumor cells (5×10^6 cells/mL), and the other group was injected with 100 μL of DPBS containing 0.3×10^6 B16F10 tumor cells (3×10^6 cells/mL). Tumor size was measured three times per week using digital calipers, and tumor volume was calculated as the long axis × the short axis^2 × 0.5. When the tumors reached a size of

200 - 300 mm³, approximately two weeks after injection, the mice were euthanized, and the tumors were harvested for flow cytometry.

2.2.2. B16F10 and B16-OVA abscopal mouse model

In this study, C57BL/6 mice were divided into two groups. The first group was injected subcutaneously in the left thigh with 100 μL of DPBS containing 0.5 × 10^6 B16-OVA tumor cells (5 × 10^6 cells/mL), while the second group was injected with 100 μL of DPBS containing 0.3 × 10^6 B16F10 tumor cells (3 × 10^6 cells/mL). Three days later, both groups were injected with 100 μL of DPBS containing 0.3 x 10^6 B16F10 tumor cells (3 × 10^6 cells/mL) in the opposite thigh. Tumor sizes were measured three times per week using calipers. When the primary tumor reached 200 - 300 mm³ and the secondary tumor reached 100 - 200 mm³, IR was administered. IR was delivered using the X-Rad 320 (Precision X-Ray, USA) at 320 kVp and 12.5 mA with 2.0 mm Al filtration at a dose rate of 4.76 cGy/sec. Following IR, mice were administered 200 μg of either isotype control antibody or αPD-1 (RMP1-14, BioXCell, USA) antibody via intraperitoneal injection. Tumor size was measured three times per week using calipers until day 22 after primary tumor implantation, and euthanasia was performed if the tumor size exceeded 2000 mm³ at any point during the experiment. In the abscopal model, flow cytometry analysis was performed three days after IR. Mice were euthanized, and tumors were harvested for flow cytometry to analyze immune cell populations and their functional states.

2.2.3. FTY720 and anti-CD8α treatment in mouse model

FTY720 (SML0700, Sigma-Aldrich, USA), commonly known as Fingolimod, was administered intraperitoneally at a dose of 25 μg one day prior to IR and continued daily at a dose of 5 μg, including the day of IR, up to day 21 after primary tumor implantation. FTY720 is a sphingosine-1-phosphate receptor modulator that blocks the egress of lymphocytes from lymphoid tissues, used in this experiment to inhibit the trafficking of T cells. This allows for the evaluation of the role of circulating T cells in mediating the abscopal effect following IR and αPD-1 therapy. To verify the efficacy of FTY720, C57BL/6 mice were treated with FTY720, and retro-orbital blood collection was performed 24 hours later. Peripheral T cell depletion was assessed by flow cytometry using

antibodies against CD3ε (145-2C11), CD4 (OKT4), CD8α (53-6.7), and CD19 (1D3), along with the LIVE/DEAD Fixable Near IR Dead Cell Stain Kit.

In the abscopal mouse model with B16-OVA as the primary tumor, anti-CD8α antibody (53-6.7, BioXCell, USA) was administered intraperitoneally at a dose of 200 μg one day prior to IR and continued at the same dose three times per week following IR, while FTY720 was administered daily up to day 19 after primary tumor implantation. Anti-CD8α is a monoclonal antibody used to deplete $CD8^+$ T cells, allowing for the assessment of the specific role $CD8^+$ T cells play in mediating the abscopal effect following IR and ICIs. To verify the efficacy of the anti-CD8α antibody, C57BL/6 mice were treated with the anti-CD8α antibody, and retro-orbital blood collection was performed 24 hours later. $CD8^+$ T cell depletion was assessed by flow cytometry using antibodies against CD3ε (145-2C11), CD4 (OKT4), CD8α (53-6.7), and CD19 (1D3), along with the LIVE/DEAD Fixable Near IR Dead Cell Stain Kit.

2.3. Immunofluorescence

In experiment A, tumors of approximately 200 mm^3 were harvested from mice that had been implanted with either B16F10 or B16-OVA tumor cells. The tumor sections designated for Immunofluorescence were fixed in 4% paraformaldehyde to preserve their structure, and the tumor sections were submitted to the Pathology Laboratory at Yonsei University College of Medicine for immunohistochemical staining. The experiment was conducted as follows. tumor sections were deparaffinized in three changes of xylene, followed by rehydration in two changes of 100% ethanol, then in 95% ethanol, and finally in 70% ethanol. After rehydration, the slides were washed in distilled water. Antigen retrieval was performed using Proteinase K (DAKO S3020, USA) with a 10-minute incubation at room temperature for both CD3 and CD8α staining. Endogenous peroxidase activity was blocked using 3% hydrogen peroxide (Duksan 3059, South Korea) for 10 minutes, followed by two washes in TBS for 5 minutes each. For primary antibody staining, anti-CD3 antibody (SP162, Abcam, UK) was diluted 1:10, and anti-CD8α monoclonal antibody (53-6.7, eBioscience, USA) was diluted 1:100. Tumor sections were incubated with the primary antibodies for 1 hour at room temperature, then washed three times in TBS for 5 minutes per wash. For secondary antibody and fluorescent labeling, FITC-conjugated goat anti-rabbit IgG (H+L) (ab6717,

Abcam, UK) was used for CD3 at a 1:200 dilution, and Alexa Fluor 594-conjugated goat anti-rat IgG (H+L) (A-11007, Thermo Fisher Scientific, USA) was used for CD8α at a 1:200 dilution. The tumor sections were incubated with secondary antibodies for 30 minutes at room temperature, followed by three 5-minute washes with TBS. Finally, the slides were mounted using a DAPI-containing fluorescence mounting medium.

Immunofluorescence imaging was performed using an Olympus BX63 microscope (Olympus, Japan). The images were analyzed with CellSens Dimension software (Olympus, Japan) to quantify fluorescence intensity and assess cell distribution. Fluorescence signal detection was optimized using filters appropriate for FITC (green) and Alexa Fluor 594 (red), ensuring specificity and minimizing background noise. Additionally, a Confocal microscope LSM 700 (Carl Zeiss, Germany) was used to obtain clear images.

2.4. Flow cytometry

Tumor tissue was isolated into single cells using a Gentle MACS mechanical dissociator in the presence of DMEM. For surface staining, cells were blocked with TruStain FcX (93, BioLegend, USA) and stained with the following primary antibodies: CD3ε (145-2C11), CD8α (53-6.7), CD19 (1D3), CD40 (3/23), CD45 (30-F11), CD24 (M1/69), and TIM-3 (RMT3-23) from BD Biosciences, USA and CD4 (OKT4), PD-1 (29F.1A12), PD-L1 (10F.9G2), Ly6c (HK1.4), F4/80 (BM8), MHC II (M5/114.15.2), CD86 (GL-1), CD11b (M1/70), CD11c (N418), and CD103 (2E7) from BioLegend, USA. LIVE/DEAD Fixable Near IR Dead Cell Stain Kit was used from Invitrogen, USA. After antibody staining, the cells were incubated at 4°C for 20 minutes before further processing. For intracellular staining, cells were processed using the Foxp3/Transcription Factor Staining Buffer Set (eBioscience, USA) and stained with Ki-67 (B56), GzmB (GB11), and Foxp3 (FJK-16s) from BD Biosciences, USA, as well as TCF-1/TCF7 (C63D9) from Cell Signaling Technology, USA. The cells were incubated for 20 minutes at room temperature. For intracellular cytokine stain, single cell suspensions were treated with Cell Stimulation Cocktail (00-4970-03, Invitrogen, USA) at 37°C for 1 hour and incubated with Protein Transport Inhibitor (00-4980-03, Invitrogen, USA) at 37°C for 4-5 hours. Cells were stained with IFN-γ (XMG1.2) and TNF-α (MP6-XT22) from eBioscience, Thermo Fisher Scientific, USA, and IL-2 (JES6-5H4) from BioLegend, USA. The cells were

incubated for 20 minutes at room temperature. Absolute cell counts were determined via flow cytometry using CountBright absolute counting beads (Invitrogen, USA) according to the manufacturer's instructions and calculated using the specified formula. Flow cytometry was performed on Lyric System (BD, USA) and output was analyzed using FlowJo software (BD, USA). Flow cytometry gating of T cells **(Fig. 1a)**, dendritic cells (DCs), tumor-associated macrophages (TAMs) **(Fig. 1b)** was performed as follows.

2.5. TCR sequencing analysis

TCR sequencing was performed on groups from the abscopal model implanted with tumor cells of different immunogenicity (B16F10, B16-OVA) that were either treated with αPD-1 alone or in combination with IR.

DNA was extracted from mouse tumors using the DNeasy Blood & Tissue Kit (Qiagen,Germany). Tumor samples were processed by adding 200 µl of Buffer AL, incubating at 56°C for 10 minutes, followed by adding 200 µl of ethanol. The mixture was transferred to a DNeasy Mini spin column and centrifuged. After washing with Buffer AW1 and Buffer AW2, the DNA was eluted with 200 µl of Buffer AE and collected by centrifugation.

T cell receptor variable beta chain sequencing: The CDR3 regions of human TCRβ chains were sequenced using Adaptive Immunosequencing (Adaptive Biotechnologies, USA). Extracted genomic DNA was amplified in a bias-controlled multiplex PCR, followed by high-throughput sequencing. Sequences were collapsed and filtered in order to identify and quantitate the absolute abundance of each unique CDR3 region for further analysis as previously described.[20,21,22]

2.6. Statistic analysis

All data were analysed at least three times. All statistical analyses were performed using GraphPad Prism 8.0 software (GraphPad Software, San Diego, CA). Data were analyzed using unpaired two-tailed t-tests for comparisons between two groups. P-values less than 0.05 were considered statistically significant. Results are presented as mean ± standard error of the mean, unless otherwise indicated.

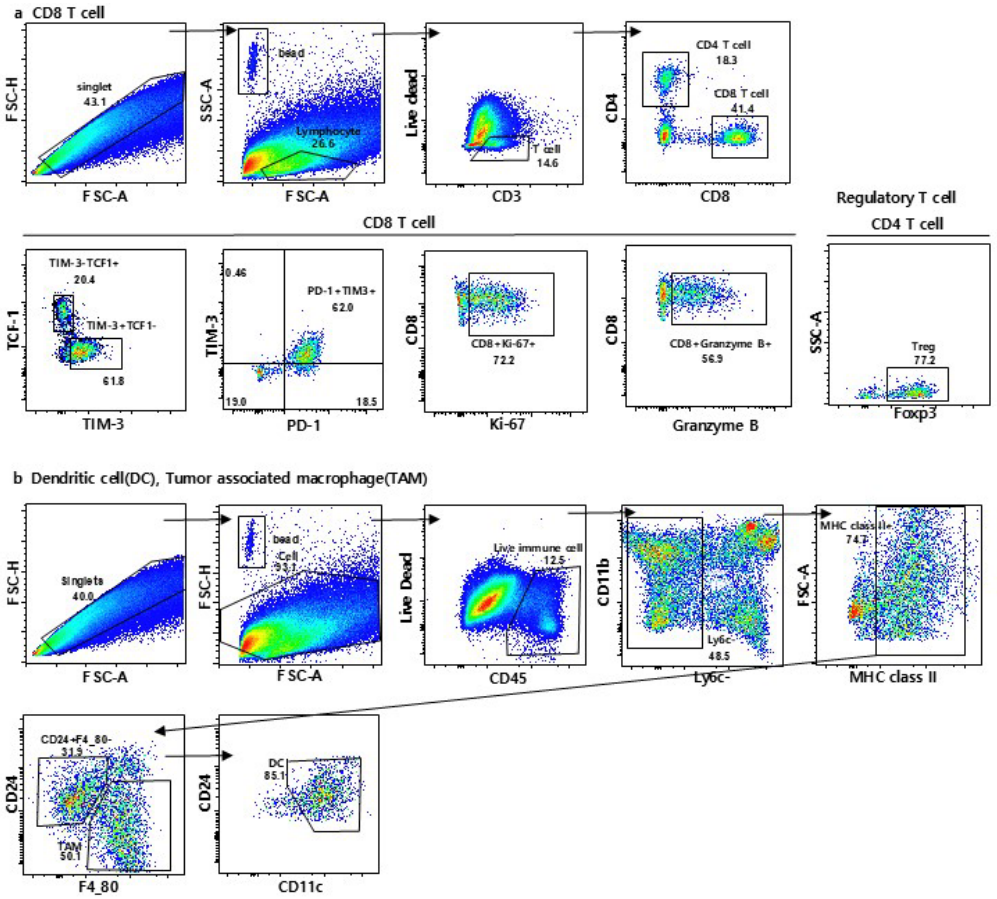

Fig 1. Gating strategy for identifying T cell, DC, TAM subpopulations

(a) Subpopulations of $CD8^+$ T cells, $CD4^+$ T cells, Tregs and the expression of TIM-3, TCF-1, Ki-67, GzmB (b) Subpopulations of DCs, TAMs

3. Results

3.1. B16-OVA exhibits the characteristics of a more immunogenic tumor compared to B16F10

Tumor immunogenicity refers to the capacity of tumors to trigger an immune response capable of suppressing or eradicating tumor growth. TME of B16 F10 and B16-OVA tumors were compared by analyzing tumor-infiltrating immune cells. Flow cytometry analysis revealed a higher frequency of T cells in B16-OVA tumors compared to B16F10 tumors **(Fig. 2a)**, with a significantly elevated number of $CD8^+$ T cells **(Fig. 2b)**. Conversely, there were no significant differences in the numbers of $CD4^+$ T cells **(Fig. 2c),** Tregs, or non-Tregs between the two tumor types **(Fig. 2d-e)**. Immunofluorescence staining revealed a significantly higher density of $CD3^+$ **(Fig. 2f, g)** and $CD8^+$ **(Fig. 2f, h)** cells in B16-OVA tumors compared to B16F10 tumors, indicating greater T cell infiltration within the B16-OVA TME. Merged images further validated increased co-localization of $CD8^+$ T cells in B16-OVA tumors **(Fig. 2f, i)**.

In addition to quantifying the number of $CD8^+$ T cells, we also examined the phenotype of $CD8^+$ T cells. B16-OVA tumors contained a significantly higher frequency of $GzmB^+$ $CD8^+$ T cells **(Fig. 2j)**, Ki-67^+ $CD8^+$ T cells **(Fig. 2k)**, and PD-1^+ $CD8^+$ T cells **(Fig. 2l)**. While there were no differences in the total numbers of DCs **(Fig. 2m)** or TAMs **(Fig. 2n)** between groups, B16-OVA tumors exhibited an increased number of $CD40^+$ DCs **(Fig. 2o)** and $CD86^+$ DCs **(Fig. 2p)** and a decreased number of PD-$L1^+$ TAMs **(Fig. 2q)**. Taken together, these findings indicate that B16-OVA tumors exhibit more immunogenic characteristics compared to B16F10 tumors.

3.2. The abscopal effect is associated with the immunogenicity of the primary tumor

We established an abscopal tumor model with differing immunogenicity in the primary tumors by using the relatively low-immunogenic B16F10 and the relatively high-immunogenic B16-OVA tumors, and subsequently examined differences in the abscopal effect by comparing the size of the secondary B16F10 tumor **(Fig.3a, b**). In the primary tumor, both the isotype and αPD-1 antibody treatment groups showed tumor growth delay upon IR **(Fig.3a, b, lower left panel**). In examining

the secondary tumor for the abscopal effect, the B16F10 abscopal model showed no significant difference **(Fig.3a, lower right panel**) between IR and non-IR groups in the isotype antibody treated condition, whereas a significant difference was observed in the B16-OVA model **(Fig.3b, lower right panel**). Additionally, in both the B16F10 and B16-OVA abscopal models, αPD-1 antibody treated groups exhibited a significant difference between IR and non-IR conditions **(Fig.3a, b**). However, the difference in secondary tumor size between IR and non-IR groups was 1.99-fold in the B16F10 model and 3.51-fold in the B16-OVA model. In summary, the B16-OVA abscopal model demonstrated a more prominent abscopal effect.

To investigate the underlying mechanisms of the enhanced abscopal effect in the B16-OVA model, which exhibits a strong abscopal effect, we utilized FTY720 to block T cell egress from lymphoid organs **(Fig.3c**). Prior to the experiment, FTY720 was administered intraperitoneally, and T cell depletion in peripheral blood was verified by flow cytometry **(Fig. 3d).** In the B16-OVA abscopal model treated with FTY720, there was a difference in tumor size between IR and non-IR tumors in the primary tumor **(Fig. 3c, lower left panel)** for both the isotype antibody and αPD-1 antibody-treated groups; however, no significant difference was observed in the secondary tumor **(Fig. 3c, lower right panel)**.

To further investigate the role of $CD8^+$ T cells, $CD8^+$ T cell depletion was performed using an anti-CD8α antibody **(Fig.3e**). Prior to the experiment, anti-CD8α was administered intraperitoneally, and $CD8^+$ T cell depletion in peripheral blood was verified by flow cytometry **(Fig. 3f)**. Similarly, in the B16-OVA abscopal model treated with anti-CD8α, a significant difference in tumor size was observed between IR and non-IR tumors in the primary tumor **(Fig. 3e, lower left panel)** for both the isotype antibody and αPD-1 antibody-treated groups; however, no significant difference was observed in the secondary tumor **(Fig. 3e, lower right panel).** These results indicate that the abscopal effect is mediated by $CD8^+$ T cells. Overall, the abscopal effect was driven by the influence of T cells, particularly $CD8^+$ T cells.

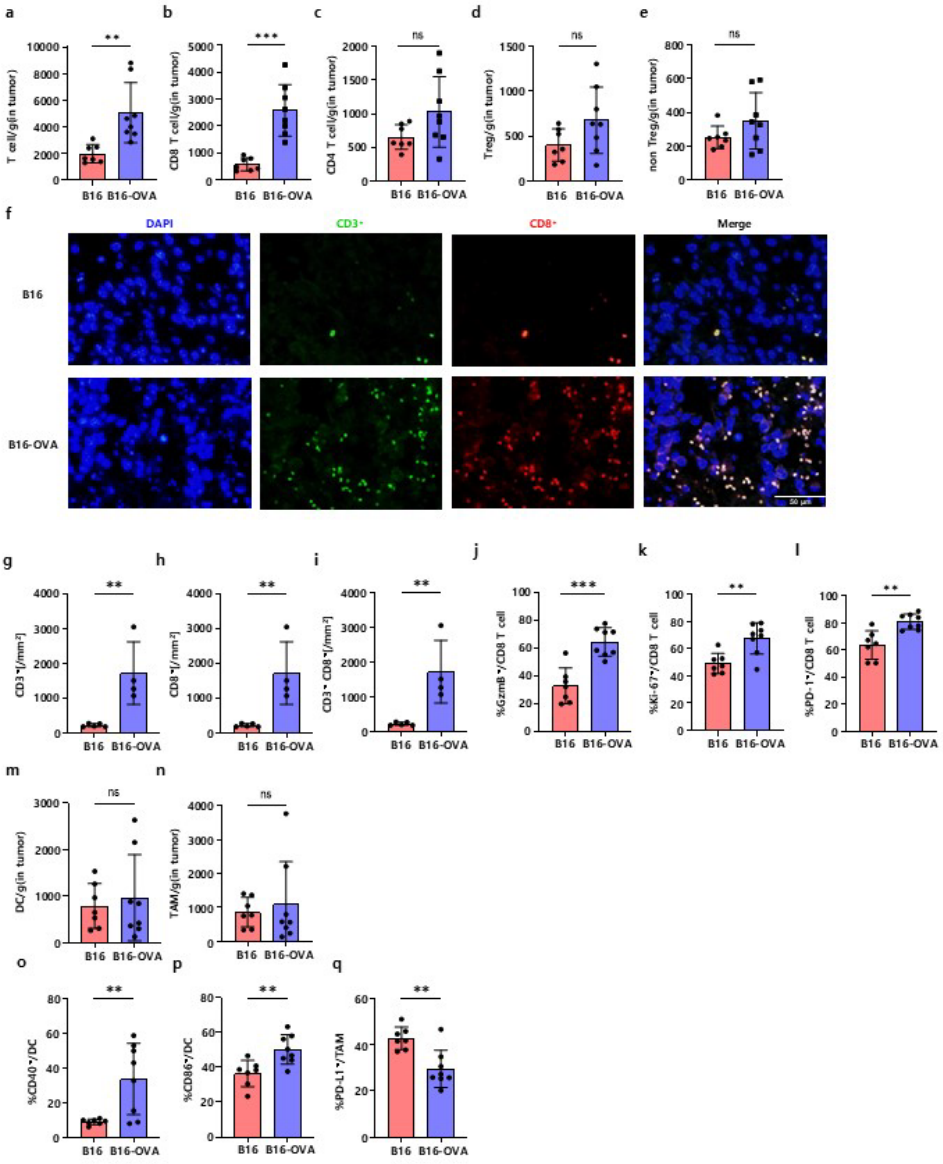

Fig 2. Number and phenotype of T cell populations in B16F10 tumors and B16-OVA tumors.
B16F10 and B16-OVA tumors, of similar size at approximately 200 mm^3, were harvested for flow cytometry to analyze immune cell populations in the TME Absolute number per g of tumor of T cell (a), $CD8^+$ T cell (b), $CD4^+$ T cell (c), Treg populations (d), non Treg populations (e). (f) Representative figure of Immunofluorescence staining results of $CD3^+$, $CD8^+$. (g) Quantification of $CD3^+$ cells per mm^2, (h) Quantification of $CD8^+$ cells per mm^2, (i) Quantification of merged $CD3^+CD8^+$ cells per mm^2. Flow cytometry showing the phenotype of $CD8^+$ T cells in B16F10 tumors and B16-OVA tumors. The proportion of $GzmB^+$ (j), Ki-67^+ (k), PD-1^+ (l) among $CD8^+$ T cells. Flow cytometry showing the phenotype of DCs (l) and TAMs (m) in B16F10 and B16-OVA tumors. The proportion of cells expressing (o) CD40 in DCs, (p) CD86 in DCs, (q) PD-L1 in DCs, (r) CD40 in TAMs, (s) CD86 in TAMs, (t) PD-L1 in TAMs (*$p<0.05$, **$p<0.01$ and ***$p<0.001$).

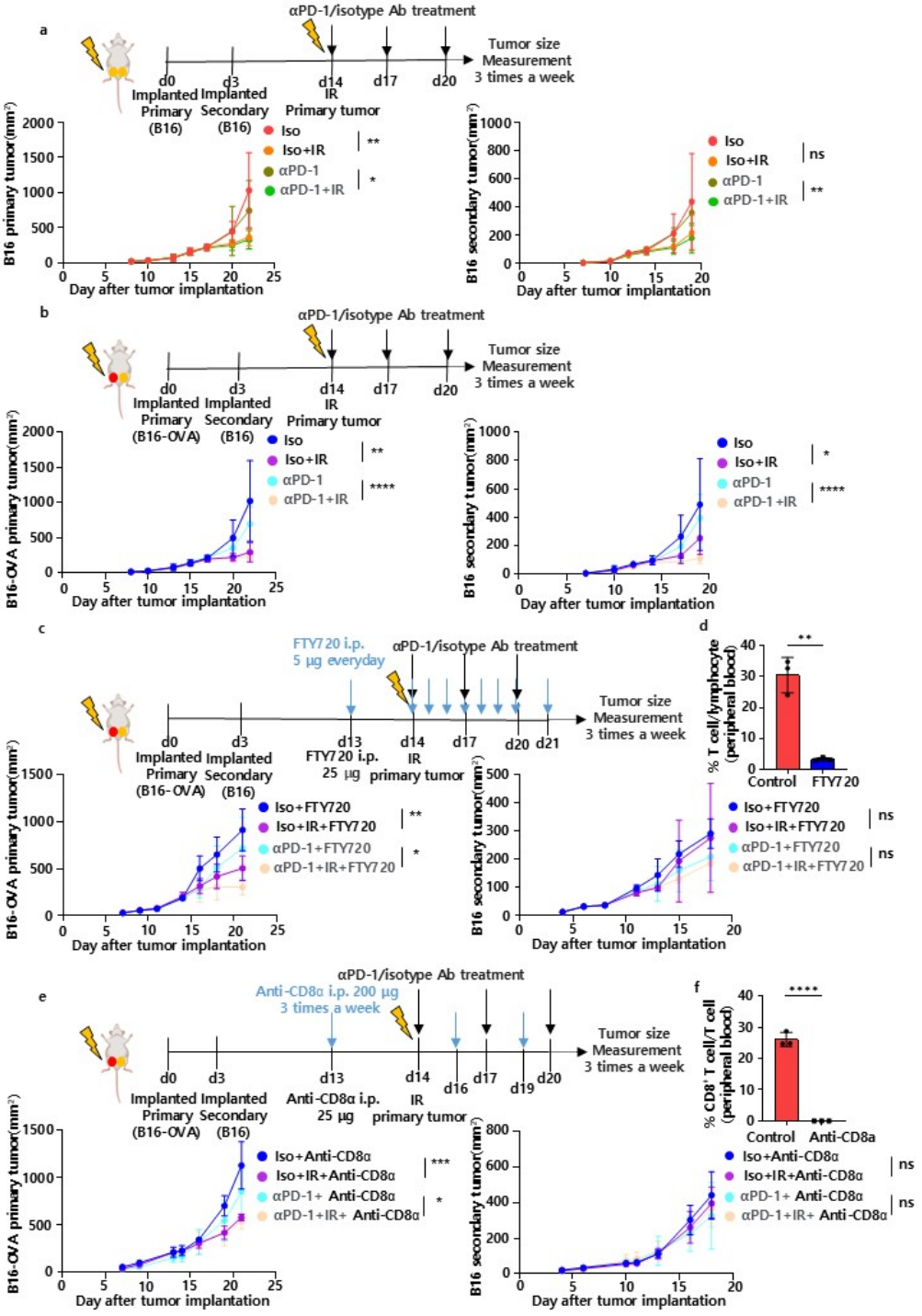

Fig 3. Experimental schedule and tumor size comparison graphs of IR and non-IR tumors following IR of tumors with differing immunogenicity in an abscopal model.

(a) A primary B16F10 tumor was implanted in the mouse's left thigh, and a secondary B16F10 tumor in the right thigh three days later (upper panel). Tumor growth curves of primary tumor (lower left panel). Tumor growth curve of seconary tumor (lower right panel).

(b) A primary B16-OVA tumor was implanted in the mouse's left thigh, and a secondary B16F10 tumor in the right thigh three days later (upper panel). Tumor growth curves of primary tumor (lower left panel). Tumor growth curve of secondary tumor (lower right panel).

(c) A primary B16-OVA tumor was implanted in the mouse's left thigh, followed by a secondary B16F10 tumor in the right thigh three days later (upper panel). FTY720 was administered intraperitoneally daily, starting the day before IR. (d) Peripheral T cell numbers measured by flow cytometry. (c) Comparison of primary tumor sizes (lower left panel). Tumor growth curve of secondary tumor (lower right panel).

(e) A primary B16-OVA tumor was implanted in the left thigh of the mouse, followed by a secondary B16F10 tumor in the right thigh three days later (upper panel). Anti-CD8α was administered every three days, starting the day before IR. (f) Peripheral $CD8^+$ T cell number measured by flow cytometry. (e) Comparison of primary tumor (lower left panel). Tumor growth curve of secondary tumor (lower right panel). Statistical analysis was performed based on the tumor size at the final measurement time point (*$p<0.05$, **$p<0.01$, ***$p<0.001$).

3.3. Increased T cell infiltration and function in the B16-OVA abscopal model

To investigate the systemic immune response to IR, we analyzed the secondary tumor. Following radiation treatment to the primary tumor, a significant increase in T cells **(Fig. 4a)** and $CD8^+$ T cells **(Fig. 4b)** was observed in the secondary tumor in IR compared to non-IR, with the exception of the B16-OVA isotype group. The increase in B16F10 $CD4^+$ T cells **(Fig. 4c)** and Tregs **(Fig. 4d)** was significantly higher in the IR group compared to the non-IR group, observed only in the αPD-1-treated B16F10 group, while non-Tregs **(Fig. 4e)** showed no significant increase. $GzmB^+$ $CD8^+$ T cells **(Fig. 4f)** showed a significant increase in the IR group compared to the non-IR group within the B16-OVA αPD-1-treated group, whereas Ki-67^+ **(Fig. 4g)**, PD-1^+ **(Fig. 4h)**, and PD-1^+TIM-3^+ **(Fig. 4i)** $CD8^+$ T cells did not show a significant increase. Notably, TCF-1^+ TIM-3^- $CD8^+$ PD-1^+ T cells **(Fig. 4j)** significantly decreased in the IR group compared to the non-IR group in both the B16-OVA isotype and αPD-1 groups. In contrast, TCF-1^- TIM-3^+ $CD8^+$ PD-1^+ T cells **(Fig. 4k)** increased in both groups, indicating differentiation from stem-like T cells to terminally exhausted T cells. Specifically in the B16-OVA αPD-1 group, TCF-1^- TIM-3^+ $CD8^+$ PD-1^+ T cells exhibited higher GzmB expression compared to TCF-1^+ TIM-3^- $CD8^+$ PD-1^+ T cells **(Fig. 4l).** These findings suggest increased differentiation of TCF-1^+TIM-3^- stem like cells to terminally differentiated cytotoxic TCF-1^-TIM-3^+ populations. TCR sequencing analysis of DNA from secondary tumors showed no significant differences in Simpson clonality across treatment groups **(Fig. 4m)**.

In the primary tumor, total T cell counts **(Fig. 4n)** did not show a significant increase in the IR group compared to the non-IR group. However, the counts of $CD8^+$ T cells **(Fig. 4o)**, $CD4^+$ T cells **(Fig. 4p)**, Tregs **(Fig. 4q)**, and non-Tregs **(Fig. 4r)** were all significantly elevated in the IR group compared to the non-IR group within the B16F10 αPD-1 treatment group. No significant increase in the frequencies of $GzmB^+$ **(Fig. 4s)**, Ki-67^+ **(Fig. 4t)**, PD-1^+ **(Fig. 4u)**, or PD-1^+TIM-3^+ **(Fig. 4v)** $CD8^+$ T cells was observed in the IR group compared to the non-IR group.

Next, we evaluated T cell function. In the secondary tumor, the number of IFN-γ^+ $CD8^+$ T cells was increased in the IR group compared to the non-IR group, except in the B16-OVA isotype group **(Fig. 5a, c)**. In the B16-OVA group, TNF-α^+ **(Fig. 5a, d)** and IL-2^+ **(Fig. 5a, e)** $CD8^+$ T cells were increased in the secondary tumor in the IR group compared to the non-IR group. In the B16-OVA

αPD-1 group, polyfunctional $CD8^+$ T cells co-expressing TNF-α^+, IL-2^+, and IFN-γ^+ were significantly increased in the secondary tumor in the IR group compared to the non-IR group **(Fig. 5a, f)**. For $CD4^+$ T cells, both the B16-OVA αPD-1 and B16 αPD-1 groups showed an increase in the number of IFN-γ^+ cells in the IR group compared to the non-IR group **(Fig. 5b, g)**. However, only the B16-OVA αPD-1 group exhibited an increase in the number of TNF-α^+ **(Fig. 5b, h)** and IL-2^+ **(Fig. 5b, i)** $CD4^+$ T cells in the IR group compared to the non-IR group. In the secondary tumor of the B16-OVA αPD-1 group, the IR group showed an increase in the number of $CD4^+$ T cells co-expressing all three cytokines compared to the non-IR group **(Fig. 5b, j)**. Collectively, polyfunctional $CD8^+$ and $CD4^+$ T cells were more effectively induced in the B16-OVA model.

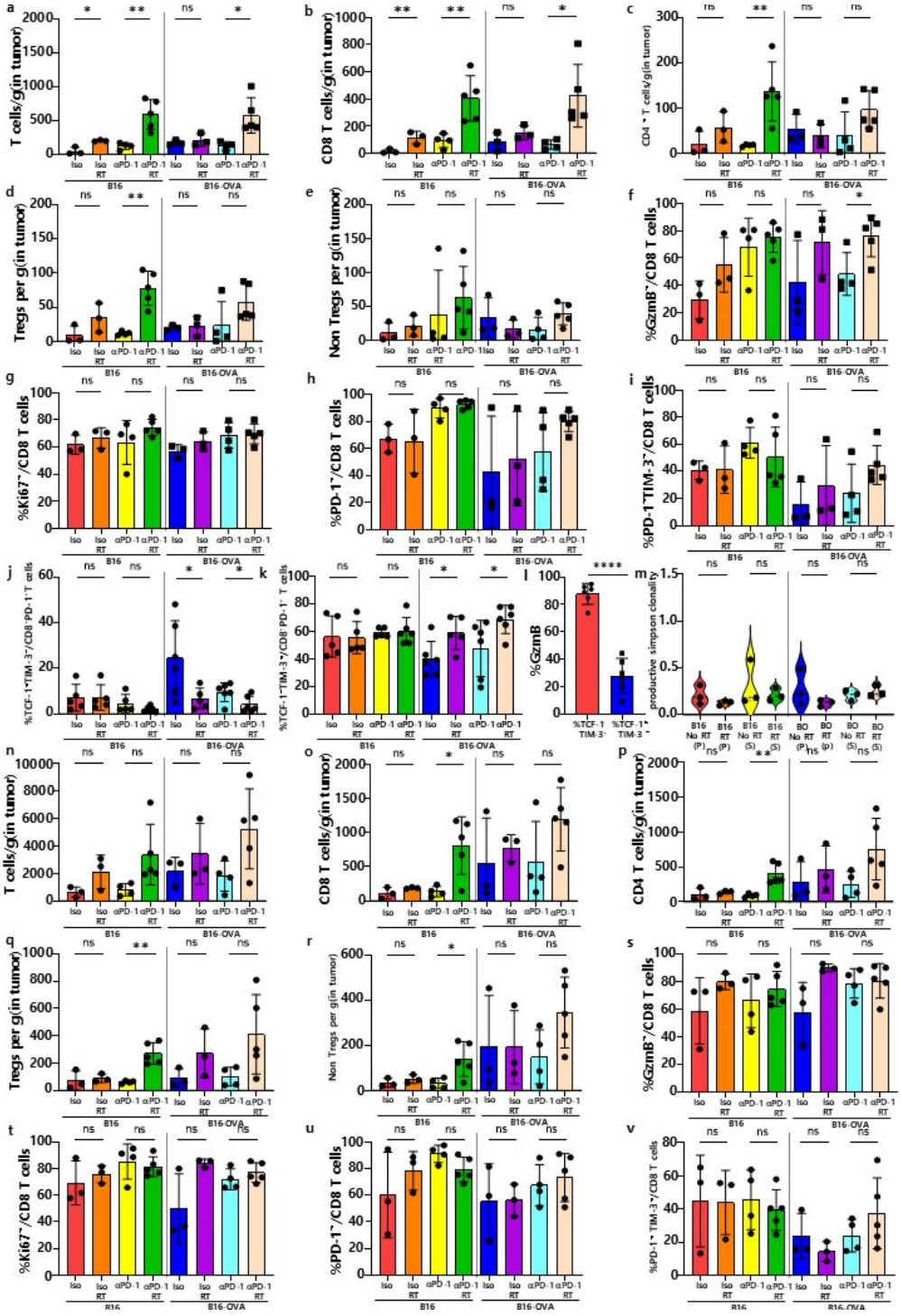

Fig 4. Flow cytometry analysis of T cell number and phenotype of secondary and primary tumors.

Flow cytometry analysis results of T cell populations and phenotype in secondary tumors (a-m) and primary tumors (n-v) from the abscopal model. Flow cytometry results for the secondary B16 tumor: (a) Number of T cells/g, (b) Number of $CD8^+$ T cells/g, (c) Number of $CD4^+$ T cells/g, (d) Number of Tregs/g, (e) Number of Non-Tregs/g. The proportion of cells expressing (f) $GzmB^+$, (g) $Ki\text{-}67^+$, (h) $PD\text{-}1^+$ among $CD8^+$ T cells. (i) The proportion of $PD\text{-}1^+TIM\text{-}3^+$ cells among $CD8^+$ T cells. The proportion of (j) $TIM\text{-}3^-TCF\text{-}1^+$, (k) $TIM\text{-}3^+TCF\text{-}1^-$ cells among $CD8^+PD\text{-}1^+$ cells. (l) Comparison of the proportion of $GzmB^+$ $CD8^+$ T cells between $CD8^+$ $PD\text{-}1^+$ $TCF\text{-}1^+$ $TIM\text{-}3^-$ and $CD8^+$ $PD\text{-}1^+$ $TCF\text{-}1^-$ $TIM\text{-}3^+$ cells in the B16-OVA abscopal group treated with combined αPD-1 and radiation. (m) Productive Simpson clonality derived from TCR sequencing between B16F10 and B16-OVA tumors in abscopal mouse model. Flow cytometry results for the primary B16F10 or B16-OVA tumor: (n) Number of T cells/g, (o) Number of $CD8^+$ T cells/g, (p) Number of $CD4^+$ T cells/g, (q) Number of Tregs/g, (r) Number of Non-Tregs/g. The proportion of cells expressing (s) GzmB, (t) Ki-67, (u) PD-1 among $CD8^+$ T cells. (v) The proportion of cells co-expressing $PD\text{-}1^+TIM\text{-}3^+$ among $CD8^+$ T cells ($^*p < 0.05$, $^{**}p < 0.01$, and $^{***}p < 0.001$).

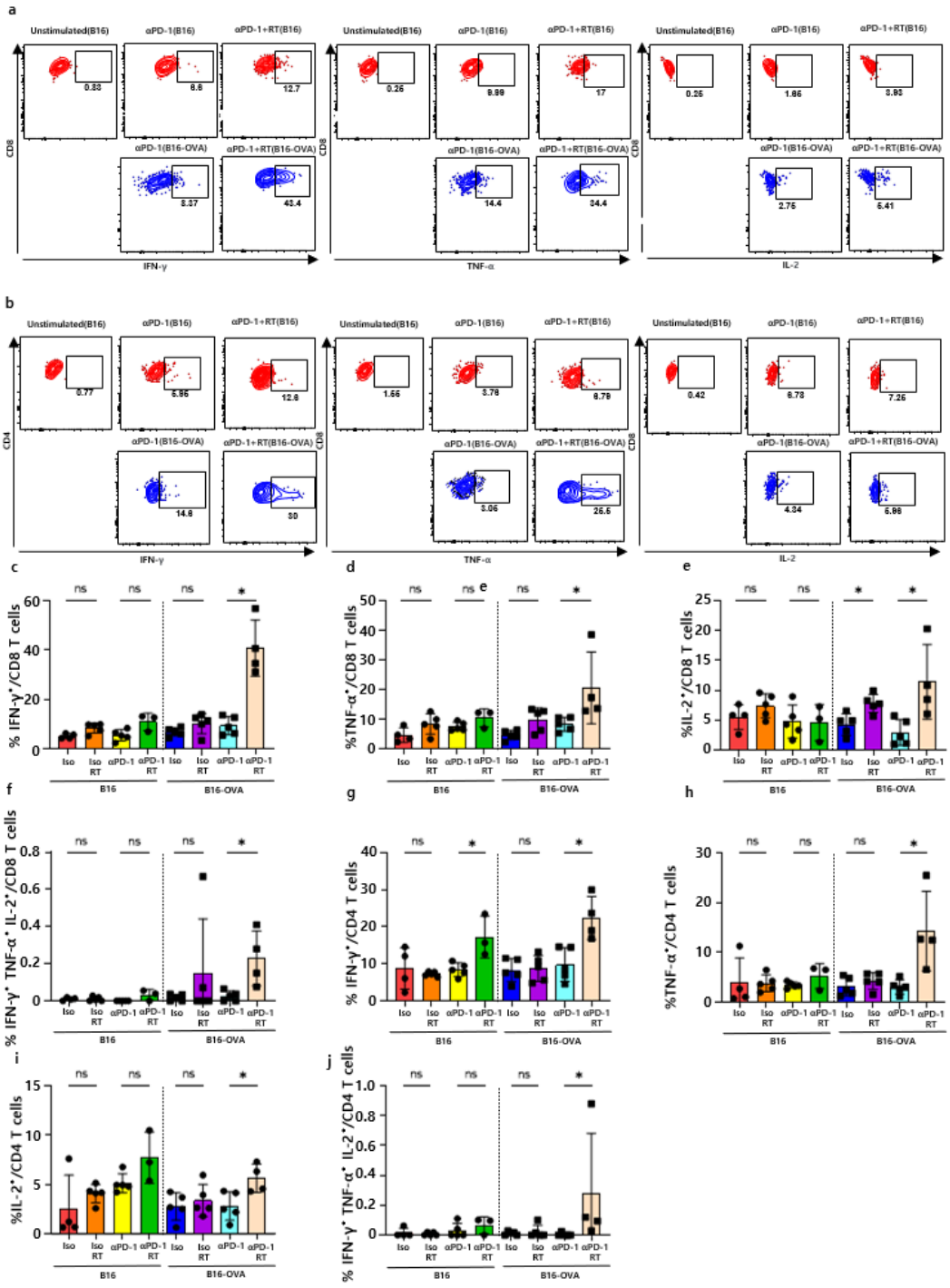

Fig 5. Flow cytometry analysis of cytokine production in secondary tumor.

Representative plot of cytokine expression in $CD8^+$ T cells (a) and $CD4^+$ T cells (b). The proportion of (c) IFN-γ^+, (d) TNF-α^+, (e) IL-2^+, (f) IFN-γ^+TNF-α^+IL-2^+ cells among $CD8^+$ T cells. The proportion of (f) IFN-γ^+, (g) TNF-α^+, (h) IL-2^+, (i) IFN-γ^+TNF-α^+IL-2^+ cells among $CD4^+$ T cells (*$p < 0.05$, **$p < 0.01$, and ***$p < 0.001$).

4. DISCUSSION

Building upon previous studies that primarily emphasized the synergistic effects of IR and ICIs, this research further underscores the critical role of intrinsic tumor immunogenicity in determining the abscopal effect. By using tumors with the same genomic background but distinct immunogenic profiles, this approach minimizes variables related to tumor-specific characteristics such as growth rate, metabolic properties, or histological differences. This enables a more direct comparison of immune responses driven solely by differences in immunogenicity, reducing potential confounding factors in data interpretation. The intrinsic immunogenicity of tumors, as exemplified by the B16-OVA model, plays a crucial role in enhancing the abscopal effect by improving the overall functionality of $CD8^+$ T cells in secondary tumors. This includes an increase in cytotoxic $CD8^+$ T cells and enhanced cytokine secretion, reflecting a more effective anti-tumor immune response. Furthermore, the improved functionality of $CD8^+$ T cells, marked by elevated GzmB expression and enhanced effector activity, provides valuable insights into the immunological mechanisms underpinning the abscopal effect. IR and ICIs not only augment T cell numbers but also enhance their effectiveness by improving their cytotoxic capabilities and cytokine production, emphasizing their central role in amplifying systemic anti-tumor immune responses. These findings underscore the importance of tumor immunogenicity and $CD8^+$ T cell-mediated immunity in achieving robust abscopal effects.

The pivotal role of tumor immunogenicity in driving the abscopal effect has been well-demonstrated. By comparing two tumor models with distinct immunogenicities—MC38 (high immunogenicity) and B16F10 (low immunogenicity)—this research emphasized that tumors with higher immunogenicity are more likely to exhibit enhanced $CD8^+$ T cell infiltration and activation, which are critical for mediating the abscopal effect. While this study effectively highlighted the correlation between tumor immunogenicity and $CD8^+$ T cell-mediated systemic responses, it primarily focused on the degree of T cell infiltration and activation, with limited exploration of $CD8^+$ T cell functional maturation or diverse cytokine-secreting capacities. In contrast, our study addressed these limitations by using the same tumor type, B16F10, with distinct immunogenic profiles (B16F10 vs. B16-OVA). This approach minimized confounding factors related to differences in

tumor-specific characteristics, such as growth rate or metabolic properties, allowing us to isolate the independent role of immunogenicity in driving the abscopal effect. Our findings revealed that the highly immunogenic B16-OVA model not only facilitated greater $CD8^+$ T cell infiltration but also significantly enhanced their functional maturation and diverse cytokine-secreting capabilities. Specifically, we observed increased Granzyme B expression and simultaneous production of cytokines such as IFN-γ, TNF-α, and IL-2, indicative of robust cytotoxic and immune-modulatory activity. Moreover, while the previous study demonstrated that tumor immunogenicity is a key determinant of the abscopal effect, it lacked detailed evaluation of how $CD8^+$ T cells transition from stem-like states to highly cytotoxic phenotypes. Our study fills this gap by providing deeper insights into the qualitative changes in $CD8^+$ T cells and their functional capacities to mediate systemic anti-tumor responses. In conclusion, while previous research established foundational knowledge on the role of immunogenicity in radiotherapy-induced systemic effects, our study builds upon this by offering a more refined analysis of $CD8^+$ T cell functionality. By focusing on their cytotoxic differentiation and polyfunctional activation, we present a more comprehensive understanding of how tumor immunogenicity can be leveraged to optimize the abscopal effect in IR and ICIs combinations.[19]

Our findings support the growing body of evidence demonstrating that PD-1 blockade synergizes with radiotherapy to enhance abscopal effects. In our study, αPD-1 treatment significantly amplified the abscopal effect, as demonstrated by delayed tumor growth and increased $CD8^+$ T cell activation in secondary tumors. This synergistic effect can be attributed to the complementary roles of radiotherapy and αPD-1 treatment in modulating the TME. IR induces immunogenic cell death, releasing tumor-associated antigens and facilitating antigen presentation by dendritic cells, which primes T cells against tumor-specific epitopes.[23] However, the immunosuppressive TME often limits the effectiveness of this immune priming. PD-1 blockade mitigates this suppression by reversing T cell exhaustion, thereby restoring effector functions of tumor-specific $CD8^+$ T cells. Our findings are consistent with prior studies demonstrating that PD-1 signaling restricts immune activation induced by radiotherapy, while PD-1 blockade restores T cell functionality and enhances the immune response, leading to improved control of tumor growth.[24] Similarly, other research has shown that combining IR with multiple ICIs can activate distinct and complementary immune

pathways, further amplifying systemic anti-tumor responses.[23] These studies collectively underscore the importance of overcoming immune suppression within the TME to optimize the therapeutic potential of radiotherapy. Taken together, our results reinforce the pivotal role of PD-1 signaling in modulating systemic anti-tumor immunity and underscore the therapeutic potential of combining radiotherapy with immune checkpoint inhibitors to maximize the abscopal effect. In the B16F10 abscopal model treated with αPD-1, an unexpected increase in Tregs was observed in both the primary and secondary tumors, the underlying mechanisms of which remain unclear and warrant further investigation. However, this finding may provide insight into the reduced abscopal effect seen in B16F10 compared to the more immunogenic B16-OVA model, highlighting the potential role of Treg-mediated immune suppression in limiting systemic antitumor responses.

Our study highlights the critical importance of functional enhancement of $CD8^+$ T cells in driving effective systemic anti-tumor responses, even in the absence of significant differences in their infiltration between treatment groups. This aligns with previous findings, including those reported in studies combining innate immunity activation with PD-1/PD-L1 blockade, which demonstrated that such therapies enhanced $CD8^+$ T cell functionality through increased production of effector molecules like IFN-γ and TNF-α and improved immune cell interactions within the TME. For instance, it was shown that this combination therapy amplified $CD8^+$ T cell activity and improved anti-tumor immune responses in colorectal cancer models by synergistically overcoming immune suppression in the TME.[25] Similarly, our findings reveal that the observed therapeutic efficacy was predominantly mediated by functional activation of $CD8^+$ T cells, as evidenced by increased polyfunctionality and effector differentiation. This observation aligns with insights from previous study, which highlighted the central role of $CD8^+$ T cell functionality in driving the abscopal effect. The study demonstrated that the quality of $CD8^+$ T cell responses, particularly their ability to produce multiple effector cytokines like IFN-γ, TNF-α, and IL-2, was crucial for effective systemic tumor control. These results mirror our findings, where therapeutic efficacy was closely associated with the enhanced polyfunctionality and effector differentiation of $CD8^+$ T cells. This underscores the importance of assessing not only the quantity but also the quality of $CD8^+$ T cell responses in evaluating immune-based therapies.[26] Future studies should aim to further enhance these functional capabilities, particularly within immune-suppressive TME, to maximize therapeutic outcomes.

Our findings suggest that $CD8^+PD1^+$ T cells, which are thought to represent tumor-specific T cells, undergo significant functional activation and differentiation following IR, particularly in the B16-OVA model. This aligns with observations from previous studies, which reported that $CD8^+PD1^+$ T cells are tumor-specific but often exhibit functional exhaustion within the TME. In those studies, $CD8^+PD1^+$ T cells were shown to express high levels of exhaustion markers, limiting their cytotoxic potential.[27] In our study, we observed that $TCF1^-TIM\text{-}3^+$ subsets of $CD8^+PD1^+$ T cells, indicative of a more cytotoxic phenotype, were significantly increased in secondary tumors following IR in the B16-OVA model. This increase was accompanied by enhanced differentiation into cytotoxic effector cells, marked by elevated expression of GzmB and other effector molecules. Interestingly, this phenomenon was exclusive to the more immunogenic B16-OVA tumors, with minimal changes observed in the B16 model. These results suggest that IR provides a strong pro-inflammatory signal that enhances the functionality of tumor-specific T cells, but this effect is more pronounced in tumors with higher immunogenicity. These findings align with observations reported in studies of other tumor models, such as diffuse large B-cell lymphoma. For instance, previous study demonstrated that $PD\text{-}1^+TIM\text{-}3^+$ T cells represent a functionally exhausted subset within the TME but retain the potential for cytotoxic activity, as indicated by their high expression of cytotoxic molecules. This supports our findings by highlighting the potential of $TIM\text{-}3^+$ subsets of tumor-infiltrating T cells to differentiate into effective cytotoxic effectors when appropriately stimulated, such as by IR.[28] Together, these results emphasize the importance of tumor immunogenicity and the activation of cytotoxic T cell subsets in optimizing the therapeutic potential of IR and immune modulation.

In clinical settings, the abscopal effect remains rare, despite strong preclinical evidence supporting its potential with combined IR and ICIs. Key barriers include the immunosuppressive TME, characterized by Treg infiltration, TAM polarization, and elevated PD-L1 expression, all of which hinder systemic immune activation. Additionally, patient-specific factors such as tumor immunogenicity, pre-existing T cell infiltration, and variability in immune competence further complicate outcomes. IR parameters, such as timing, dose, and sequencing with ICIs, play a crucial role in influencing the induction of systemic immune responses. These factors are known to impact the effectiveness of IR in promoting the abscopal effect.[29] Addressing these challenges through optimized treatment strategies and biomarker integration is critical to realizing the full potential of

the abscopal effect in clinical practice.[12] Our findings underscore the critical role of tumor immunogenicity in determining the efficacy of the abscopal effect, highlighting the need for predictive tools to optimize therapeutic strategies Recent advancements in radiomics have provided valuable insights into non-invasive methods for assessing tumor immune profiles. Radiomics features extracted from CT imaging have been shown to reliably predict $CD8^+$ T cell infiltration and immune activity, offering a non-invasive biomarker for evaluating tumor immune profiles and predicting responses to ICIs.[30] Notably, previous study demonstrated that radiomics signatures derived from CT imaging can predict $CD8^+$ T cell infiltration and immune activity within tumors. In this study, radiomics features, including tumor shape, texture, and intensity, were extracted from CT images to construct a radiomics signature. The signature was correlated with immunohistochemical data, specifically $CD8^+$ T cell distribution, confirming its reliability as a biomarker for tumor immune infiltration. Furthermore, the radiomics signature was shown to predict responses to anti-PD-1/PD-L1 immunotherapy, emphasizing the link between high $CD8^+$ T cell infiltration and enhanced therapeutic outcomes. Imaging-based biomarkers, such as radiomics signatures, have demonstrated strong correlations with immune activity markers, including $CD8^+$ T cell infiltration, providing a reliable tool for predicting responses to ICIs in combination with IR.[31] These findings underscore the utility of CT-based radiomics in evaluating tumor-infiltrating lymphocytes and their association with treatment responsiveness.[30] Our findings align with previous radiomics research. This study demonstrated that radiomics biomarkers derived from CT imaging reliably correlated with CD8 expression and immune activity, highlighting their utility in identifying immune "hot" tumors likely to respond to immunotherapy. Similarly, in our study, tumors with higher immunogenicity, such as B16-OVA, exhibited a more robust abscopal effect mediated by enhanced $CD8^+$ T cell functionality and differentiation following IR. These findings underscore the potential of radiomics biomarkers to stratify tumors by immunogenicity, enabling personalized radiotherapy and immunotherapy strategies to maximize systemic immune activation.[32]

5. CONCLUSION

In conclusion, this study highlights the critical role of tumor immunogenicity in enhancing the abscopal effect and promoting systemic anti-tumor responses, with $CD8^+$ T cell cytokine production

playing a pivotal role. We found that highly immunogenic tumors, such as B16-OVA, fostered greater CD8+ T cell infiltration and elevated cytokine expression, particularly IFN-γ, TNF-α, and IL-2, which likely contributed to improved tumor control following IR and αPD-1 antibody therapy. Building on these findings, irradiating a highly immunogenic tumor may increase the likelihood of inducing an abscopal effect, primarily mediated through T cell-dependent mechanisms. These results hold significant implications for clinical strategies aiming to optimize radiotherapy (RT) targets in combination with immune checkpoint blockade. By prioritizing the irradiation of tumors with higher immunogenic profiles, it may be possible to enhance systemic immune activation and improve therapeutic outcomes, especially in metastatic settings where systemic control is crucial.

REFERENCES

1. Sia, Joseph, et al. "Molecular mechanisms of radiation-induced cancer cell death: a primer." *Frontiers in cell and developmental biology* 8 (2020): 41.

2. Galluzzi, Lorenzo, et al. "Consensus guidelines for the definitsion, detection and interpretation of immunogenic cell death." *Journal for immunotherapy of cancer* 8.1 (2020).

3. Motwani, Mona, Scott Pesiridis, and Katherine A. Fitzgerald. "DNA sensing by the cGAS–STING pathway in health and disease." *Nature Reviews Genetics* 20.11 (2019): 657-674.

4. Sharabi, Andrew B., et al. "Stereotactic radiation therapy augments antigen-specific PD-1–mediated antitumor immune responses via cross-presentation of tumor antigen." *Cancer immunology research* 3.4 (2015): 345-355.

5. Lhuillier, Claire, et al. "Radiotherapy-exposed $CD8^+$ and $CD4^+$ neoantigens enhance tumor control." *The Journal of clinical investigation* 131.5 (2021).

6. Demaria, Sandra, and Silvia C. Formenti. "Role of T lymphocytes in tumor response to radiotherapy." *Frontiers in oncology* 2 (2012): 95.

7. Lee, Youjin, et al. "Therapeutic effects of ablative radiation on local tumor require CD8+ T cells: changing strategies for cancer treatment." *Blood, The Journal of the American Society of Hematology* 114.3 (2009): 589-595.

8. Formenti, Silvia C., and Sandra Demaria. "Systemic effects of local radiotherapy." *The lancet oncology* 10.7 (2009): 718-726.

9. Demaria, Sandra, et al. "Ionizing radiation inhibition of distant untreated tumors (abscopal effect) is immune mediated." *International Journal of Radiation Oncology* Biology* Physics* 58.3 (2004): 862-870.

10. Suek, Nathan, et al. "Targeted APC activation in cancer immunotherapy to enhance the abscopal effect." *Frontiers in immunology* 10 (2019): 604.

11. Rödel, Franz, et al. "Contribution of the immune system to bystander and non-targeted effects of ionizing radiation." *Cancer letters* 356.1 (2015): 105-113.

12. Turchan, William Tyler, Sean P. Pitroda, and Ralph R. Weichselbaum. "Radiotherapy and immunotherapy combinations in the treatment of patients with metastatic disease: current status and future focus." *Clinical Cancer Research* 27.19 (2021): 5188-5194

13. Proietto, Marco, et al. "Tumor heterogeneity: preclinical models, emerging technologies, and future applications." *Frontiers in Oncology* 13 (2023): 1164535.

14. Formenti, Silvia C., and Sandra Demaria. "Combining radiotherapy and cancer immunotherapy: a paradigm shift." *JNCI: Journal of the National Cancer Institute* 105.4 (2013): 256-265.

15. Sato, Hiro, et al. "DNA double-strand break repair pathway regulates PD-L1 expression in cancer cells." *Nature communications* 8.1 (2017): 1751.

16. Zhou, Zhaokai, et al. "Infiltrating treg reprogramming in the tumor immune microenvironment and its optimization for immunotherapy." *Biomarker Research* 12.1 (2024): 97.

17. Deng, Liufu, et al. "Irradiation and anti–PD-L1 treatment synergistically promote antitumor immunity in mice." *The Journal of clinical investigation* 124.2 (2014): 687-695.

18. Wei, Joyce, et al. "Sequence of αPD-1 relative to local tumor irradiation determines the induction of abscopal antitumor immune responses." *Science immunology* 6.58 (2021): eabg0117.

19. Lai, Jin-Zhi, et al. "Abscopal effects of local radiotherapy are dependent on tumor immunogenicity." *Frontiers in Oncology* 11 (2021): 690188.

20. Robins HS, et al. Comprehensive assessment of T-cell receptor β-chain diversity in αβ T cells. Blood 114(19):4099-4107. (2009)

21. Carlson CS, et al. Using synthetic templates to design an unbiased multiplex PCR assay. Nature Communications 4:2680. (2013)

22. Robins HS, et al. Ultra-sensitive detection of rare T cell clones. J. Immunol. Methods 375(1-2):14-9. (2012)

23. Twyman-Saint Victor, Christina, et al. "Radiation and dual checkpoint blockade activate non-redundant immune mechanisms in cancer." *Nature* 520.7547 (2015): 373-377.

24. Park, Sean S., et al. "PD-1 restrains radiotherapy-induced abscopal effect." *Cancer immunology research* 3.6 (2015): 610-619.

25. Xie, Qi, et al. "Cellular mechanisms of combining innate immunity activation with PD-1/PD-L1 blockade in treatment of colorectal cancer." *Molecular Cancer* 23 (2024): 252.

26. Wang, Xueying, et al. "Abscopal effect: from a rare phenomenon to a new frontier in cancer therapy." *Biomarker Research* 12.1 (2024): 98.

27. Ahmadzadeh, Mojgan, et al. "Tumor antigen–specific CD8 T cells infiltrating the tumor express

high levels of PD-1 and are functionally impaired." *Blood, The Journal of the American Society of Hematology* 114.8 (2009): 1537-1544.

28. Roussel, Mikaël, et al. "Functional characterization of PD1+ TIM3+ tumor-infiltrating T cells in DLBCL and effects of PD1 or TIM3 blockade." *Blood Advances* 5.7 (2021): 1816-1829.

29. Buchwald, Zachary S., et al. "Radiation, immune checkpoint blockade and the abscopal effect: a critical review on timing, dose and fractionation." *Frontiers in oncology* 8 (2018): 612.

30. Sun, Roger, et al. "A radiomics approach to assess tumour-infiltrating CD8 cells and response to anti-PD-1 or anti-PD-L1 immunotherapy: an imaging biomarker, retrospective multicohort study." *The Lancet Oncology* 19.9 (2018): 1180-1191.

31. Sun, Roger, et al. "Radiomics to predict outcomes and abscopal response of patients with cancer treated with immunotherapy combined with radiotherapy using a validated signature of CD8 cells." *Journal for Immunotherapy of Cancer* 8.2 (2020).

32. Aoude, Lauren G., et al. "Radiomics biomarkers correlate with CD8 expression and predict immune signatures in melanoma patients." *Molecular Cancer Research* 19.6 (2021): 950-956.

Abstract in Korean

종양 면역원성에 따른 압스코팔 효과의 차이와 방사선 치료 효능 증대 방안에 대한 연구

압스코팔 효과는 방사선을 통해 항종양 반응을 증강시키며, 종양의 면역원성에 따라 다르게 나타날 수 있다. 본 연구는 B16 종양 세포와 더 면역원성이 높은 B16-OVA 종양 세포주를 비교하여 이러한 차이를 조사했다. 마우스의 왼쪽 허벅지에 B16 또는 B16-OVA 종양 세포를 이식하고, 오른쪽 허벅지에 B16 종양 세포를 이식하여 압스코팔 효과를 관찰했다. 방사선 조사 및 αPD-1 치료에 따라 8개의 실험군을 설정하였으며, 생쥐는 왼쪽 허벅지에 10 Gy의 방사선 용량을 받고, αPD-1은 이틀 간격으로 복강 주사로 투여되었다. 유세포 분석을 통해 종양 미세환경 내 면역 세포의 표현형과 기능을 평가하였고, TCR 염기서열 분석을 통해 T세포 수용체의 클론 구성을 분석했다.

결과적으로 면역원성이 더 높은 B16-OVA 종양 세포는 B16 종양 세포보다 더 두드러진 압스코팔 효과를 나타냈다. 이 효과는 방사선이 조사되지 않은 종양에서 $CD8^+$ T 세포 침투가 증가하고, GzmB, Ki-67, IFN-γ, TNF-α, IL-2의 발현이 높아져 면역 반응의 다기능성을 증가시키는 것과 관련이 있었다. 또한, B16-OVA 방사선 조사된 생쥐의 방사선이 조사되지 않은 종양 세포에서 수지상 세포의 CD40 발현이 더 높게 나타났다. 이러한 면역 반응의 차이에도 불구하고 치료 그룹 간의 T세포 수용체 클론 구성에는 유의미한 변화가 없었다. 본 연구는 종양 면역원성이 압스코팔 효과에 중요한 역할을 하며, 면역원성이 높을수록 더 강한 체내 면역 반응을 유도함을 시사한다. 이러한 결과는 방사선 치료와 면역 치료를 결합할 때 종양의 면역원성을 고려하여 압스코팔 효과를 최적화하고 치료 결과를 향상시키는 전략 설계의 중요함을 강조한다.

핵심되는 말 : 압스코팔 효과, 면역원성, 이온화 방사선